pISSN 1229-3008 eISSN 2287-6251
Progress in Superconductivity and Cryogenics
Vol.24, No.4, (2022), pp.29~35 https://doi.org/10.9714/psac.2022.24.4.029

Superconductivity of HTS REBCO coated conductors with multi-superconducting layers

Ye Rim Lee[a], Kyu Jeong Song*[, a], Gwan Tae Kim[b], Sang Soo Oh[b], and Hong Soo Ha[b]

[a] *Div. of Sci. Education and Institute of Sci. Education, Jeonbuk National University, Jeonju, 54896 Korea*
[b] *Superconductivity Research Center, Korea Electrotechnology Research Institute, Changwon, 51543 Korea*

(Received 28 November 2022; revised or reviewed 20 December 2022; accepted 21 December 2022)

Abstract

We fabricated MHOS (multi-HTS layers on one substrate) high-temperature superconducting (HTS) REBCO conductors using HTS REBCO coated conductor (CC) A-specimen, which induces an artificial magnetic flux pinning effect, and HTS REBCO CC B-specimen, that does not induce this effect. The superconducting magnetic properties of the fabricated MHOS conductors were examined by measuring their magnetic moment $m(H)$ curves using a physical property measurement system (QD PPMS-14). The critical current density (J_c) characteristics of our four-layered MHOS HTS REBCO conductor specimens such as BAAB, BBBB, and AAAA were lower than those of their two-layered and three-layered counterparts. At a temperature T of 30 K the magnetic flux pinning physical indicator δ values (obtained from the relationship $J_c \propto H^{-\delta}$) of the three-layer ABA (δ = 0.35) and two-layer AB (δ = 0.43) specimens were found to be significantly lower than those of the four-layer ABBA (δ = 0.51), BAAB (δ = 0.60), AAAA (δ = 0.78) and BBBB (δ = 0.81) structures.

Keywords: MHOS HTS Conductor, magnetic moment, critical current density, irreversible magnetization, magnetic flux pinning physical indicator

1. INTRODUCTION

After the discovery of high-temperature superconductors with ceramic oxide compounds in 1986 [1], many research groups have made efforts to develop high-temperature superconducting (HTS) conductors as a replacement for copper wires. The first generation BSCCO PIT (powder-in-tube) tapes were developed in the 1990s [2-4]. The BSCCO PIT tapes, however, showed disadvantages of using Ag sheath materials that were too costly to produce and significant deterioration in their critical current characteristics when exposed to high magnetic fields. Despite these shortcomings, the development of BSCCO PIT tapes, which have a bit economical and somewhat improved in superconducting critical current characteristics, were led by a company, and they were commercialized in the 2000s and are available for purchase today [5, 6]. The main conditions of HTS conductors suited to the development of HTS magnets (the most marketable and important application of HTS conductors), are their high superconducting critical current and excellent mechanical strength in high-magnetic field environments. Therefore, researchers have subsequently continued to develop HTS magnets using HTS REBCO coated conductors (CCs), which are comparatively economical to produce and possesses excellent superconducting critical current characteristics in a high magnetic field and strong mechanical strength. The development of second-generation HTS REBCO CCs has continued since the mid-1990s. Eventually, the HTS REBCO CCs have developed and commercialized since the 2000s in Korea and out Korea, and they are available for purchase today [7-9].

The critical current density J_c of HTS REBCO CCs is high, but the engineering current density J_e is low as the superconducting layer occupies less than 5% of the HTS REBCO CCs. Various methods have been developed to increase J_e, some that significantly reduce the thickness of substrate structures other than the superconducting layer, and some that increase the thickness of the superconducting layer. The former is particularly difficult as it requires the development of new substrate structures; increasing the thickness of the HTS REBCO layer is the more technologically achievable. The superconducting layer in commercially available HTS REBCO CCs is 1 ~ 1.5 μm thick. Once this layer exceeds 1.5 μm, it becomes increasingly porous as the deposition temperature on the surface of the superconducting layer lowers, thereby diminishing its superconducting properties [10, 11]. In an attempt to prevent this degradation, many research groups have applied a technique that maintains a suitable deposition temperature on the surface of the superconducting layer regardless of its thickness, successfully developing ~ 5 μm thick HTS REBCO CCs with a superconducting critical current density J_c of 1000 A/cm or more [11-13]. However, through this technology it is not easy to develop an HTS REBCO CC with a long length of several hundred meters or more which was improved the engineering current density J_e by ~ 3 times.

* Corresponding author: songkj@jbnu.ac.kr

An alternative method of increasing J_e requires a multilayer HTS REBCO CC. Recently, a Korean research group developed an MHOS (multi-HTS layers on one substrate) HTS REBCO conductor with a high J_e that consists of several superconducting layers on a single substrate [14-15]. To achieve this, the REBCO superconducting layer was first separated from the HTS REBCO CC, after which the separated superconducting layers were repeatedly stacked by Ag-diffusion heat treatment [14-15]. A long-length MHOS HTS REBCO conductor is currently under development by the same team.

In this study, two types of HTS REBCO CCs (one that introduces and one that does not introduce an artificial magnetic flux pinning effect) were used to fabricate MHOS HTS REBCO conductors with either two superconducting layers, three superconducting layers, or four superconducting layers. The basic superconducting magnetic properties of the prepared specimens were investigated using a physical property measurement system (PPMS-14). For each MHOS HTS REBCO conductor, we assessed the critical current density J_c, the physical indicator δ representing the magnetic flux pinning effect, the irreversibility magnetic field H_{irr} (which is an important factor for the application of the superconducting wire to an electric power system), and the second magnetic flux state-transition-magnetic field H_2 (the position at which the applied magnetic field induces magnetic fluxes to begin to deviate from the collective behavior) [16].

2. EXPERIMENTAL PROCEDURE

Two types of HTS REBCO CCs were prepared to fabricate various MHOS HTS REBCO conductors. One was an HTS REBCO CC ('A tape') that introduces an artificial magnetic flux pinning effect, while the other was an HTS REBCO CC ('B tape') that does not. Using the prepared A and B tapes, we fabricated various MHOS HTS REBCO conductors: AB (with two superconducting layers), ABA (with three superconducting layers), and AAAA, BBB, ABBA, and BAAB (with four superconducting layers). Additional details concerning the applicable preparation methods are provided in previous papers [14, 15]. Fig. 1 is a schematic diagram shows the structures of the produced conductors. Each section comprised of blue vertical lines represents an A superconducting layer, while each section comprised of red horizontal lines represents a B superconducting layer. In total, eight specimens (two types of HTS REBCO CCs and six types of MHOS HTS REBCO conductors) were prepared. We investigated the basic magnetic superconducting properties of each using a physical property measurement system (QD, PPMS-14T equipment) installed at Seoul National University. All specimens were ~ 3 mm × ~ 3 mm to enable PPMS measurement. We then measured magnetic moment $m(H)$ curves by assessing increases and decreases in the magnetic field at a fixed temperature.

Each specimen was placed in the PPMS measurement position so that the direction of the applied magnetic field

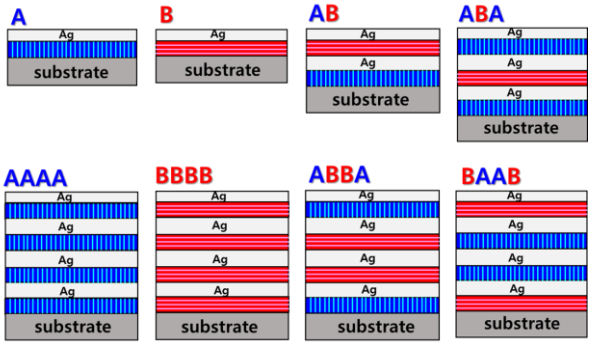

Fig. 1. Schematic of the two HTS REBCO CCs and six MHOS HTS REBCO CCs.

and the *c*-axis direction of the specimen were parallel to each other. Magnetic moment $m(H)$ curves were then measured at a fixed temperature of 10 K interval from 10 K to 50 K and of 5 K interval from 50 K to 90 K. The magnetic moment $m(H)$ curves were then measured as the magnetic field was increased from 0 G to 12 T, and again as the magnetic field was decreased from 12 T to 0 G.

Normal state background magnetic moment $m(H)$ curves were measured by increasing and decreasing the magnetic field at T = 100 K, which is higher than the critical transition temperature T_c of the REBCO superconductor. The normal state background $m(H)$ values were used as correction values for each specimen, as corrected pure superconducting state $m(H)$ values were obtained by removing the normal state background $m(H)$ values from the raw $m(H)$ values measured at the fixed temperature. The unit of measured magnetic moment m is [emu = G-cm^3]. Dividing the magnetic moment m values by the volume of the superconducting layer of the specimens yielded estimated magnetization M values and magnetization $M(H)$ curves for all specimens. The unit of the magnetization M is [emu/cm^3 = G]. In this manner, we investigated the magnetic properties of each specimen, including the two types (A and B) of HTS REBCO CC and the six types (AB, ABA, ABBA, BAAB, BBBB, and AAAA) of MHOS HTS REBCO conductor.

Irreversible magnetization ΔM data was also obtained from the magnetization $M(H)$ curve. Irreversible magnetization ΔM (= $M(H_{dec})$ - $M(H_{inc})$) is defined as the difference between the value of magnetization $M(H_{dec})$ in the decreasing field H_{dec} branch and the value of magnetization $M(H_{inc})$ in the increasing field H_{inc} branch, at a fixed each magnetic field H [16-18]. The critical current density J_c was analyzed using Bean's critical state model, $J_c = 20\Delta M/\{a[1-(a/3b)]\}$, in which a and b are the sizes of each thin film specimen, and ΔM is the irreversible magnetization [19, 20]. The magnetic flux pinning effect was determined by deriving the magnetic flux pinning physical indicator δ values from $J_c \propto H^{-\delta}$, which describes the relationship between J_c and magnetic field H [16-18, 21]. In addition, we investigated the irreversible magnetic field H_{irr} values of the irreversible magnetization $\Delta M \approx 0$, as well as the second-order flux state-transition-magnetic field H_2 values.

3. RESULTS AND DISCUSSION

The purpose of this study was to analyze the superconducting properties of MHOS HTS REBCO conductors manufactured using various combinations of HTS REBCO CC A-specimen (that induce an artificial magnetic flux pinning effect) and B-specimen (that do not induce this effect). To investigate the superconducting properties present in each of the six fabricated MHOS HTS REBCO conductors, it was necessary to compare and analyze the properties of their component A- and B-specimens. In short, we sought to confirm how these two layers, when stacked to form the MHOS HTS REBCO conductors, affect each other's superconducting properties. We therefore examined the magnetic properties of the superconducting specimens, including magnetic moment $m(H)$ curves (obtained from data measured at fixed temperatures). Pure magnetization $M(H)$ curves were derived after removing background (at T = 100 K) magnetic moment $m(H)$ values from measured raw magnetic moment $m(H)$ values, and by dividing the superconducting volume of each specimen. Fig. 2 shows the $M(H)$ curves for the HTS REBCO CC A- and B-specimens used to manufacture each of our MHOS HTS REBCO conductors. A- and B-specimens were measured at fixed temperatures (intervals of 10 K) as it increased from 10 K to 50 K and at intervals of 5 K as the temperate was raised from 50 K to 90 K. The applied magnetic field was applied parallel to the *c*-axis direction of each specimen. Further, Fig. 2 shows that the $M(H)$ curves of the A- and B-specimens are nearly vertically symmetrical, and that the ΔM values of the A-specimen are greater than those of the B-specimen. Based on these results, we predicted that the A-specimen would show superior superconducting properties to the B-specimen.

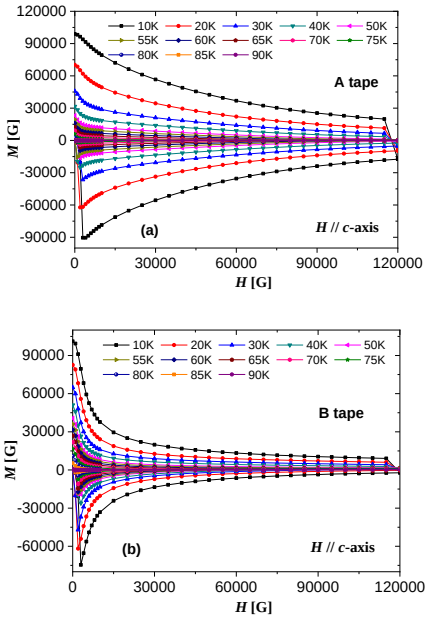

Fig. 2. Magnetization M versus magnetic field H for an (a) A-specimen and (b) B-specimen of the HTS REBCO CCs at temperatures between 10 K and 90 K, with external fields applied parallel to the *c*-axis.

Fig. 3-(a) compares the magnetization $M(H)$ curves of the A- and B-specimen at a temperature T of 30 K gathered from the magnetization $M(H)$ curves shown in Fig. 2. This figure highlights that the irreversible magnetization ΔM (= $M(H_{dec})$ - $M(H_{inc})$) values of the A-specimen are approximately twice as high as those of the B-specimen when the magnetic field H is 5000 G or higher. Fig. 3-(b) shows a log-normal scale of the critical current density J_c and the magnetic field H, that is, $\log(J_c)$ and H relationship curves of the A- and B-specimens estimated from Bean's critical state model [19, 20], $J_c = 20\Delta M/\{a[1-(a/3b)]\}$ (a and b are the size of the specimen, and ΔM is the irreversible magnetization) as applied to the same data (at T = 30 K) as that shown in Fig. 3-(a): the J_c values of the A-specimen are significantly higher than those of B-specimen in the entire region of H = 5000 G or higher. Particularly in the region of magnetic field H = 4 T or higher, A-specimen values were approximately 4 to 5 times higher than those of the B-specimen.

Fig. 3-(c) shows the log-log scale of the J_c and the H, that is, the $\log(J_c)$ and $\log(H)$ relationship graph for the data reflected in Fig. 3-(b). In this figure, the region that is fitted by the $J_c \propto H^{-\delta}$ relation of the J_c and the H, that is, the region that is shown to linearly decrease, is the region where the pinned magnetic fluxes interact with the surrounding magnetic fluxes and shows collective behaviors as the applied magnetic field increases. As a linear decreasing slope, the indication physical quantity δ values that represent the magnetic flux pinning characteristics are 0.23 for the A-specimen (which induces an artificial magnetic flux pinning effect) and 0.73 for the B-specimen (which does not). Fig. 3-(d) shows a temperature-dependent $\delta(T)$ graph for the magnetic flux pinning physical indicator δ values that reflects the collective behavior characteristics of the magnetic fluxes, when the applied field is parallel to the *c*-axis of the specimens. In the low temperature region (T = 50 K or less), which is far away from the T_c, the physical indicator δ values remain nearly constant: $\delta \sim 0.25$ for the A-specimen and $\delta \sim 0.75$ for the B-specimen. The physical indicator δ values gradually increase as T reaches and exceeds 50 K. Across the entire temperature range, the physical indicator δ value of the B-specimen is approximately 3 times that of the A-specimen. The smaller the physical indicator δ value (i.e., the smaller the magnitude of the linear decrease slope) the weaker the collective behavior characteristics of the magnetic fluxes, and the greater the magnetic flux pinning effect. Ultimately, the magnetic flux pinning effect observed from the A-specimen was ~ 3 times greater than that seen in the B-specimen.

Fig. 4-(a) shows the temperature dependence of irreversible magnetic field H_{irr} for the HTS REBCO CC A- and B-specimens. H_{irr} characteristics are basic magnetic properties important to the development of superconducting magnets and electric power devices. H_{irr} is determined as the magnetic field value where the irreversible magnetization $\Delta M \approx 0$ starts in Fig. 2. Fig. 4-(a) indicates that the irreversible magnetic field H_{irr} values of the A-specimen are somewhat higher than those of the

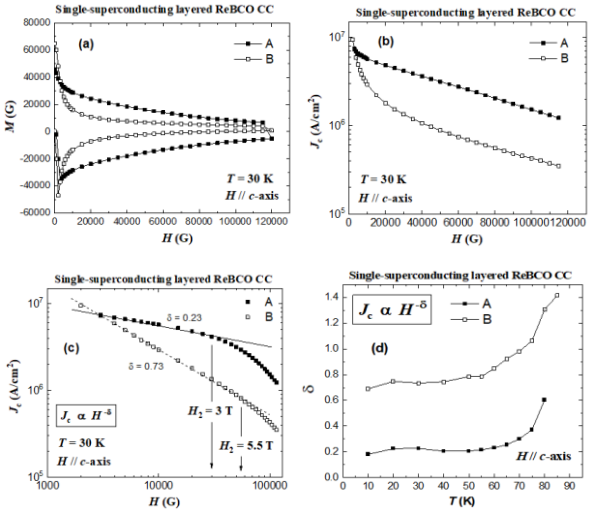

Fig. 3. (a) Magnetization M versus magnetic field H, (b) semi-logarithmic plots of the critical current density J_c versus H, and (c) the logarithmic plots of the J_c versus H for each HTS REBCO CC at a temperature of 30 K with a field H applied parallel to the c-axis, and (d) the plot of δ versus temperature T for HTS REBCO CCs with field H applied parallel to the c-axis. Solid squares represent A tape while open squares show B tape.

B-specimen below T = 80 K. In contrast, the log(J_c) and log(H) relationship graph shows that the characteristics of the phase transition of the magnetic flux moving behavior can be explained from the characteristic changes of the critical current density J_c related to the behavior of the magnetic fluxes according to the increase of the applied magnetic field [16-18]. It is possible to distinguish between the first characteristic magnetic field H_1, which is a state-transition-magnetic field that starts to decrease linearly from a constant value, and the second characteristic magnetic field H_2, which is the a state-transition-magnetic field that deviates from this linear decrease by decreasing somewhat sharply.

Fig. 3-(c) includes a region that the critical current density J_c decreases linearly as the applied magnetic field increases. The second magnetic flux state-transition-magnetic field H_2 values can be determined as follows. The region of collective behavior magnetic flux phase due to the interaction of magnetic fluxes is a linearly decreasing region from Fig. 3-(c). A region that the J_c decreases more rapidly from the linear decreasing tendency in Fig. 3-(c) represents a phase in which magnetic fluxes move freely. Accordingly, second magnetic flux state-transition-magnetic field H_2 values can be determined by identifying the field at which the J_c begins to deviate sharply from the otherwise linear decrease. At T = 30 K, the H_2 value of the A-specimen is 3 T, and that of the B-specimen is 5.5 T. Fig. 4-(b) shows $H_2(T)$ graphs that incorporate information concerning the temperature of the second magnetic flux state-transition-magnetic field H_2 values. Between T = 55 K and the T_c, the H_2 values of the A- and B-specimens are nearly identical. As the temperature falls below T = 55 K, the H_2 values of the B-specimen gradually increase relative to those of the A-specimen. We are currently exploring

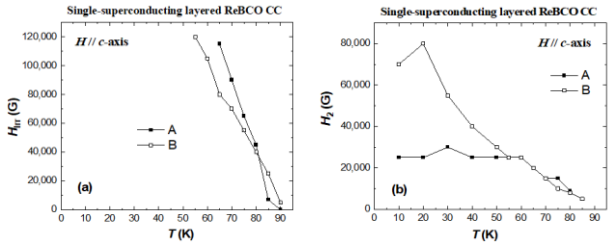

Fig. 4. Temperature dependence of (a) the irreversibility field H_{irr} and (b) the magnetic flux state transition field H_2 for HTS REBCO CCs with a field H applied parallel to the c-axis. Solid squares represent A tape while open squares represent B tape.

the mechanism that explains this phenomenon through additional studies.

Six types of MHOS HTS REBCO conductors were prepared using HTS REBCO CC A- and B-specimens: a single two-layer (AB) conductor, a single three-layer (ABA) conductor, and multiple four-layer (AAAA, BBBB, ABBA, and BAAB) conductors. Fig. 5-(a) shows the log-normal scale of the critical current density J_c, as estimated using Bean's critical state model, and the magnetic field H, i.e. log(J_c) and H relationship graphs reflecting a magnetic field applied to each specimen parallel to their c-axis at T = 30 K. Examining the semi-log $J_c(H)$ characteristics of each of the eight specimens, the A-specimen (with the artificial magnetic flux pinning effect) has the highest, and the BBBB specimen the lowest. The characteristics of the ABA specimen were lower, and those of the AAAA, BAAB, and BBBB specimens were significantly lower, than those of the B-specimen (that did not induce an artificial magnetic flux pinning effect). Fig. 5-(b) shows the log(J_c) and log(H) relationship graph using the same data as that reflected in Fig. 5-(a). The physical indicator δ values, which reflect the magnetic flux pinning characteristic, form a linear decreasing slope for each of the eight types of specimens in the region fitted with the $J_c \propto H^{-\delta}$. When T = 30 K, the values of δ fall within a range of 0.23 to 0.81. The characteristics of A (δ = 0.23), ABA (δ = 0.35), AB (δ = 0.43), ABBA (δ = 0.51), and BAAB (δ = 0.60) specimens are superior, while those of the AAAA (δ = 0.78) and BBBB (δ = 0.81) specimens are somewhat inferior, to those of B (δ = 0.73). Fig. 5-(c) shows a log-normal scale of the critical current density J_c and temperature T (log(J_c) and T relationship graphs) when the direction of the applied magnetic field is parallel to the c-axis of the specimens and the H = 2 T. Similar to the results of observed in Fig. 5-(a), the characteristics of the AAAA, BAAB, and BBBB specimens are significantly deteriorated.

Fig. 6 shows the temperature dependence δ(T) graph of the physical indicator δ values, which represent the behavior characteristics of the collective magnetic fluxes for the HTS REBCO CC A- and B-specimens as well as the six types of MHOS HTS REBCO conductors when the field is applied parallel to the c-axis of the specimens. Fig. 6 presents physical indicator δ values obtained through the processes reflected in Figs. 3-(c) and 3-(d) across the entire

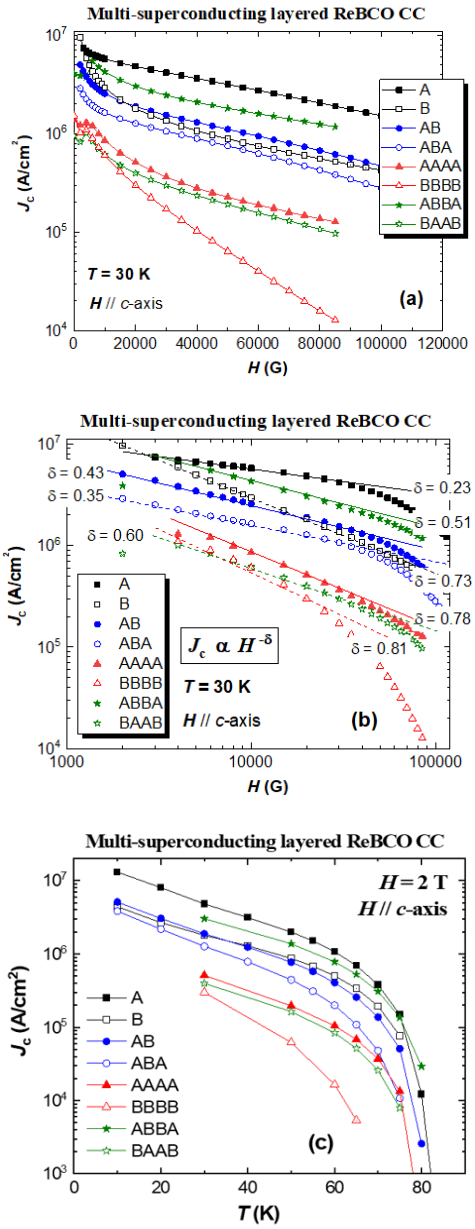

Fig. 5. (a) Semi-logarithmic plots of the critical current density J_c versus the magnetic field H, (b) logarithmic plots of J_c versus H at T = 30 K, and (c) semi-logarithmic plots of J_c versus temperature T in an applied field wherein H = 2 T, for both HTS REBCO CCs and MHOS HTS REBCO CCs when magnetic field H is applied parallel to the c-axis.

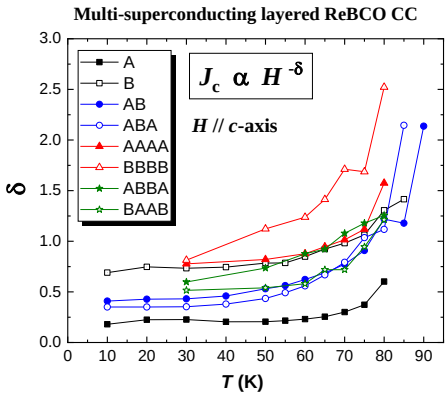

Fig. 6. Plot of the δ values versus T for both HTS REBCO CCs and MHOS HTS REBCO CCs with magnetic field H applied parallel to the c-axis.

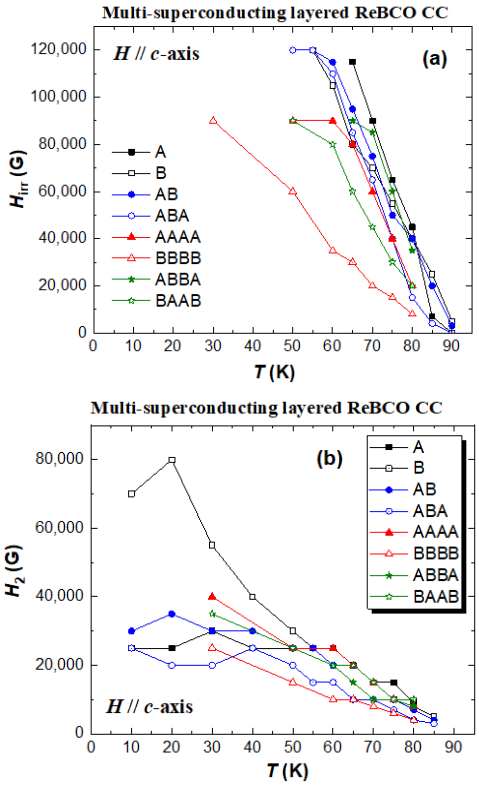

Fig. 7. Temperature dependence of (a) the irreversibility field H_{irr} and (b) the magnetic flux state transition field H_2 for both HTS REBCO CCs and MHOS HTS REBCO CCs with magnetic field H applied parallel to the c-axis.

measurement temperature range for each of the eight types of specimens. The magnetic flux behavior characteristics of the AB and ABA specimens are superior to those of the AAAA, BBBB, ABBA, and BAAB specimens.

The dependence of temperature T on the irreversible magnetic field H_{irr} and the second magnetic flux state-transition-magnetic field H_2 of the HTS REBCO CC A- and B-specimens is apparent in Fig. 4. The irreversible magnetic field H_{irr} and the second magnetic flux state-transition-magnetic field H_2 values for the MHOS HTS REBCO conductors can be obtained by applying the same method used to generate Fig. 4. Fig. 7-(a) and -(b) are $H_{irr}(T)$ and $H_2(T)$ graphs for each of the eight types of specimens; in all cases, the applied magnetic fields applied are parallel to the c-axis. Although no clear trend emerges according to the types of specimens, these graphs do confirm that the superconducting properties of the MHOS HTS REBCO conductors do not deteriorate overall.

The development of HTS magnets and electric power device applications requires improvements to the engineering current density J_e of the HTS REBCO CC. As increasing the thickness of the HTS layer is the most practical method of achieving this, MHOS HTS REBCO conductors, which are manufactured with stacked superconducting layers, are a viable alternative to

large-capacity HTS REBCO CCs. Note however, that even if the J_e is improved by a thicker high-temperature superconducting layer, it may nevertheless remain difficult to apply a large-capacity superconducting power device if the basic superconducting properties have deteriorated. Therefore, care must be taken that basic superconducting magnetic properties not be allowed to deteriorate even as J_e improves.

This study explored the characteristics of MHOS HTS REBCO conductors built using A-specimen, which introduces an artificial magnetic flux pinning effect, and B-specimen, which does not. In summary, the AAAA specimen showed significantly lower superconducting properties, including critical current density J_c and physical indicator δ (which denotes collective magnetic flux behavior), than the A-specimen; A-specimen may not have maintained its superconducting properties due to mechanical damage, such as fine cracks in the superconducting layers, that may have occurred during the manufacture of the MHOS HTS REBCO conductors, or thermal damage due to diffusion heat treatment bonding. The characteristics of the BBBB, BAAB, and AAAA specimens were significantly lower than those of the AB and ABA specimens, which suggests that mechanical and thermal damages due to the increase in time for manufacturing MHOS HTS REBCO conductors are grow seriously. Although the superconducting properties of the AB and ABA specimens were somewhat lower than those of the A-specimen, the remarkable improvement in these properties we observed, compared to the B-specimen, is very encouraging. The results of this study suggest that a suitable method of combining A-and B-specimen that minimizes mechanical and thermal damage associated with the manufacture of MHOS HTS REBCO conductors is possible. This combination enables the manufacture of large-capacity MHOS HTS REBCO conductors with a high J_e while avoiding any degradation of basic magnetic superconducting properties.

4. SUMMARY

Six types of MHOS (multi-HTS layers on one substrate) HTS (high-temperature superconducting) REBCO conductors were fabricated using HTS REBCO CC (coated conductor) A-specimen (which induces an artificial magnetic flux pinning effect) and HTS REBCO CC B-specimen (that does not). The superconducting magnetic properties of six MHOS HTS REBCO conductors (with AB, ABA, ABBA, BAAB, BBBB, and AAAA superconducting layers) were compared with those of HTS REBCO CC A- and B-specimens. We measured the magnetic moment $m(H)$ curves of two types of HTS REBCO CC A- and B-specimens and six MHOS HTS REBCO conductors using a PPMS (physical property measurement system) and investigated various superconducting magnetic properties using the $m(H)$ data. In general, the superconducting properties of the A-specimen were remarkably superior to those of the B-specimen. The critical current density J_c characteristic of A-specimen was 4~5 times higher than that of the B-specimen, and the magnetic flux pinning effect characteristic of the A-specimen (δ = 0.23) was superior to that of the B-specimen (δ = 0.73) as T = 30 K. The δ(T) characteristics of the A-specimen remained superior across the entire temperature range. The critical current density J_c characteristics of the BAAB, AAAA, and BBBB four-layer specimens were substantially reduced, while their magnetic flux pinning physical indicator δ values (BAAB (δ = 0.60 at T = 30K), AAAA (δ = 0.78 at T = 30K), and BBBB (δ = 0.81 at T = 30K)) suggested somewhat worse performance than the ABA (δ = 0.35 at T = 30K) and AB (δ = 0.43 at T = 30K) specimens. Compared to the MHOS HTS REBCO conductors with a four-layer structure, the overall critical current density characteristics of the two-layer AB and three-layer ABA structures were good, while their δ(T) characteristics were excellent (~ 0.4). Based on these results, we conclude that either AB or ABA structures are the most suitable for the further development of MHOS HTS REBCO conductors.

ACKNOWLEDGMENT

This work was supported by a grant from the Basic Science Research Program, administered through the National Research Foundation of Korea (NRF) and funded by the Ministry of Education (NRF-2021R1A2C1094771), as well as the Research Program at Jeonbuk National University.

REFERENCES

[1] J. G. Bednorz and A. K. Muller, "Possible high Tc superconductivity in the Ba-La-Cu-O system," *Z. Phys. B*, vol. 64, pp. 189-193, 1986.

[2] K. Heine, J. Tenbrink, and M. Thoner, "High-field critical current densities in $Bi_2Sr_2Ca_1Cu_2O_{8+x}$/Ag wires," *Appl. Phys. Lett*., vol. 55, pp. 2441, 1989.

[3] A. P. Malezemoff, Q. Li, and S. Fleshler, "Progress in BSCCO-2223 tape technology," *Physica C*, vol. 282-287, no. 1, pp. 424-427, 1997.

[4] A. R. Moodenbaugh, M. Suenaga, L. H. Lewis, D. E. Cox, M. W. Rupich, G. N. Riley, Q. Li, and R. Parrella, "Superconducting critical current densities and synchrotron X-ray diffraction measurements of (Bi, Pb)$_2$Sr$_2$Ca$_2$Cu$_3$O$_y$/Ag composite," *Physica C*, vol. 377, pp. 67, 2002.

[5] Sumitomo Electric Home Page, "DI-BSCCO Dynamically Innovative Bi-2223 wire," Accessed: Nov. 20, 2022. [Online]. Available: http://www.sumitomoelectric.com/super/wire

[6] T. Nakashima, S. Kobayashi, T. Kagiyama, K. Yamazaki, M. Kikuchi, et al., "Overview of the recent performance of DI_BSCCO wire," *Cryogenics*, vol. 52, pp. 713-718, 2012.

[7] SuNAM Home Page, "SuNAM 2G HTS wire specification," Accessed: Nov. 20, 2022. [Online]. Available: http://www.i-sunam.com

[8] SuperPower Home Page, "SuperPower 2G HTS wire specification," Accessed: Nov. 20, 2022. [Online]. Available: http://www.superpower-inc.com/content/2G-hts-wire

[9] C. Senatore, C. Barth, M. Bonura, M. Kulich, and G. Mondonico, "Field and temperature scaling of the critical current density in commercial REBCO coated conductor," *Supercond. Sci. Technol.*, vol. 29, pp. 014002, 2016.

[10] Q. X. Jia, S. R. Flotyn, P. N. Arendt, and J. F. Smith, "High-temperature superconducting thick films with enhanced

supercurrent carrying capability," *Appl. Phys. Lett*., vol. 80, pp. 1601, 2002.

[11] S. R. Flotyn, et al., "Materials science challenges for high-temperature superconducting wire," *Nature Mater.*, vol. 6, pp. 631-642, 2007.

[12] R. Pratap, et al., "Growth of High-Performance Thick Film REBCO Tapes Using Advanced MOCVD," *IEEE Trans. Appl. Supercond*., vol. 29, no. 5, pp. 6600905, 2019.

[13] A. Markelov, A. Valikov, V. Chepicov, A. Petrzhik, P. Degtyarenko, et al., "2G HTS wire enhanced engineering current density attained through the deposition on HTS layer with increased thickness," *Progress in Superconductivity and Cryogenics*, vol. 21, no. 4, pp. 29-33, 2019.

[14] Hongsoo Ha, Gwantae Kim, Hyunwoo Noh, Jaehun Lee, Seunghyun Moon, and Sang-Soo Oh, " Fabrocation of 1 m long multi layered superconducting coated conductor with high engineering critical current density," *Supercond. Sci. Technol*., vol. 33, no. 4, pp. 044007, 2020.

[15] Gwantae Kim, Hongsoo Ha, Hosup Kim, Sangsoo Oh, Jaehun Lee, and Seunghyun Moon, "Fabrication of 6-superconducting layered HTS wire for high engineering critical current density," *Progress in Superconductivity and Cryogenics*, vol. 23, no. 4, pp. 10-13, 2021.

[16] Seok Han Yang and Kyu Jeong Song, "The Superconducting Properties of a High-Temperature Superconducting GdBCO-Coated Conductor," *New Physics: Sae Mulli*, vol. 68, no. 12, pp. 1293-1301, 2018

[17] Kyu Jeong Song, Seok Han Yang, Gi Ppeum Choi, Jichon Lim, and Chan Park, "The Magnetic Properties of Several HTS GdBCO-Coated Conductors," *IEEE Trans. Appl. Supercond*., vol. 29, no. 5, pp. 6601204, 2019.

[18] J. S. You, J. H. Yang, and K. J. Song, "Superconductivity for HTS GdBCO CC with heat treatment," *Progress in Superconductivity and Cryogenics*, vol. 23, no. 1, pp. 12-16, 2021.

[19] C. P. Bean, "Magnetization of high-field superconductors," *Rev. Mod. Phys*., vol. 36, pp. 31-36, 1964.

[20] X. L. Wang, A. H. Li, S. Yu, S. Ooi, K. Hirata, et al., "Thermally assisted flux flow and individual vortex pinning in $Bi_2Sr_2Ca_2Cu_3O_{10}$ single crystals grown by the traveling solvent floating zone technique," *J. Appl. Phys*., vol. 97, pp. 10B114, 2005.

[21] S. Kang, A. Goyal, J. Li, A. A. Kapud, P. M. Martin, et al., "High-Performance High-Tc Superconducting Wires," *Science*, vol. 311, no. 5769, pp. 1911-1914, 2006.